Motor strength classification with machine learning approaches applied to anatomical neuroimages

Francesco Bardozzo
Neuronelab, DISA-MIS
Università degli Studi di Salerno
Salerno, Italy
fbardozzo@unisa.it

Sebastian Cano Uribe
Neuronelab, DISA-MIS
Università degli Studi di Salerno
Salerno, Italy
Faculty of Engineering - UTP
Pereira, Colombia
sebastiancanouribe@utp.edu.co

Andrea G. Russo
DIPMED
Università degli Studi di Salerno)
Salerno, Italy
andrusso@unisa.it

Mateo Jiménez Castaño
Neuronelab, DISA-MIS
Università degli Studi di Salerno
Salerno, Italy
Faculty of Engineering - UTP
Pereira, Colombia
mjimenez@utp.edu.co

Mattia Delli Priscolli
Neuronelab, DISA-MIS
Università degli Studi di Salerno
Salerno, Italy
mdellipriscoli@unisa.it

Fabrizio Esposito
DIPMED
Università degli Studi di Salerno
Salerno, Italy
faesposito@unisa.it

Roberto Tagliaferri
Neuronelab, DISA-MIS
Università degli Studi di Salerno
Salerno, Italy
robtag@unisa.it

***Abstract*—Pattern recognition methods for classification are leveraged in the field of computational anatomy and neuroimaging showing high reliability and applicability. Body-brain human functions related to the motor-strength features can be discovered by data integration and analysis of 3D brain images, phenotype and behavioural information. This work is focused on the study of feature-based interplay of 3D brain structures with motor-strength information. In particular, this research introduces an ensemble of supervised machine learning approaches for a binary motor-strength classification (strong vs weak) based on 3D brain anatomical features. The proposed approach has been evaluated on 1113 case studies by obtaining well-defined features and reaching the average accuracy of 72% on the test set.**

***Index Terms*—Pattern recognition, motor-strength, machine learning, classification, feature extraction.**

I. Introduction

In the last decades, integrative and statistical data analysis of body-brain related human functions have been based on high-dimensional data sets of magnetic resonance images (MRI) in combination with phenotypic and behavioural information [1]. Nowadays, machine learning and deep learning methodologies are able to underline unknown aspects of the structure and functioning of the living brain and their relations with human body [2]. A central role in these type of studies is the reduction of dimensionality which derives from big-data analysis. Particularly, machine learning feature extraction methods can be applied to select the most important features of the set, leading to a substantial reduction in data dimensionality [3]. In addition, classical methodologies based on pattern recognition for classification are being applied successfully in the field of computational anatomy showing high reliability and usability. Thus, this work is focused on the study of feature-based multivariate interplay of 3D brain structures with phenotypic motor-strength information. In particular, an ensemble of supervised machine learning approaches for motor-strength classification based on brain anatomical features are introduced [4]–[8].

The latest and most advanced methodologies for feature extraction in neuroimaging can provide high levels of recognition accuracy with acceptable performance over time [10]. According to many scientists in the literature, it is possible to distinguish different subject conditions or between patients and controls with machine learning and deep learning approaches based on the features extracted from the neural substrates. For example, *Lavagnino et al.* introduce a methodology based on Lasso for the identification of anorexia nervosa signs [11]; moreover, *Akhila et al.* show neural networks based methodologies for dementia detection [12]; finally, *Shen et al.* provide random-forest based strategies for the representation of the different fatigue stages [13].

This work is focused on the study of feature-based interplay of 3D brain structures with motor-strength information. In particular, an ensemble of supervised machine learning approaches for a binary motor-strength classification (strong

978-1-7281-6926-2/20/$31.00 ©2020 IEEE

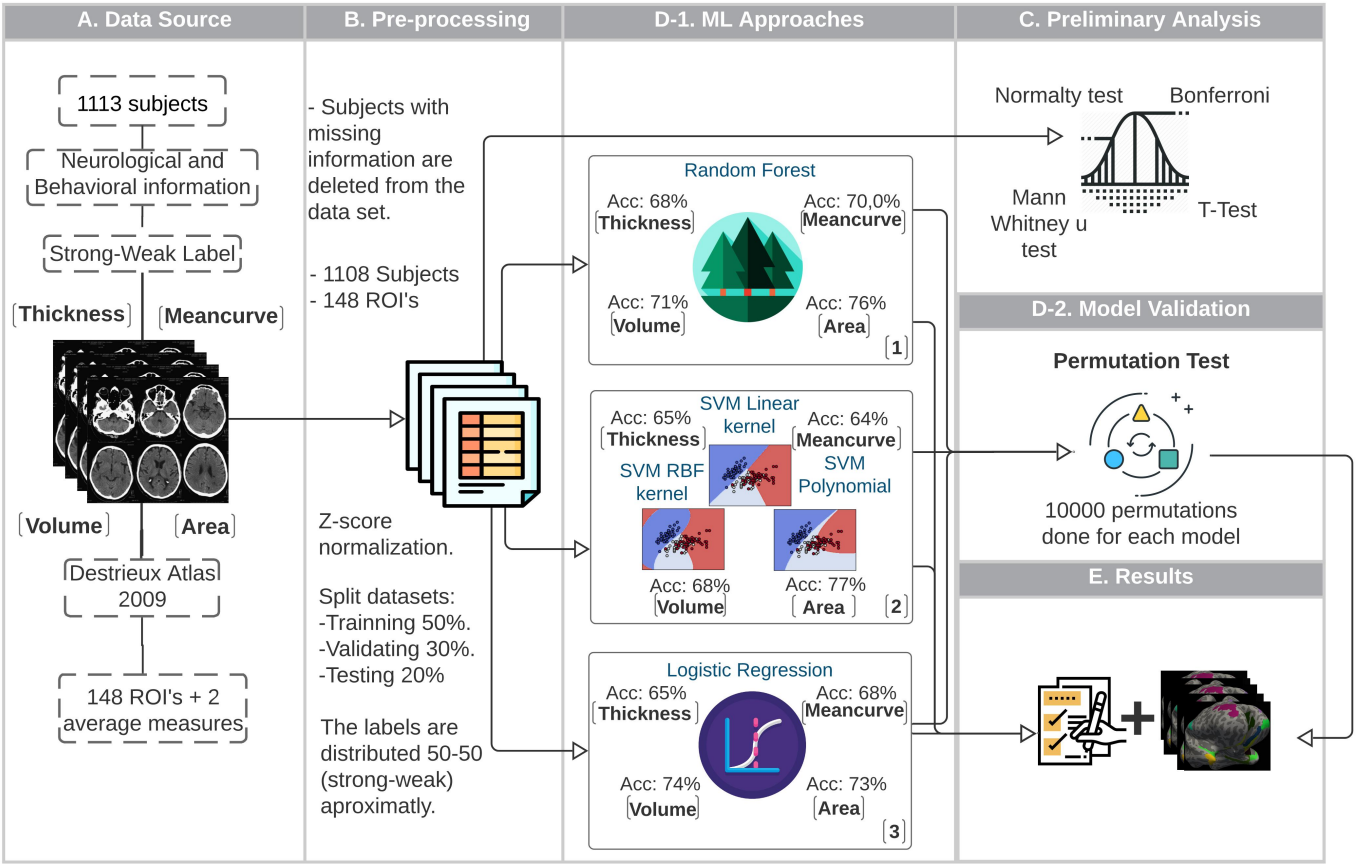

Fig. 1. In Fig. 1 an overview of this work is provided. The boxes in the figure are numbered with letters so that they correspond to the letters of the paragraphs and sub-paragraphs in the text. In box **A**, the process of data elicitation is described. In particular, neurological information and behavioural labels are extracted and integrated with the Destrieux Atlas [9]. In box **B** the preprocessing step is described. In particular, missing values are removed, then the dataset is normalized and split into train, test and validation. Some parametric tests are applied to analyze data distributions (box **C**). In box **D-1**, the models of ML employed in this work are shown (*(1)* Random Forest, *(2)* Support Vector Machine with 3 Kernels (SVM Linear, SVM RBF, SVM Polynomial) and *(3)* Logistic Regression). ML results are validated with 10.000 permutation tests (box **D-2**). Relevant results are summarized and displayed in Table II and III and in Fig. 2 (see also box **E**).

vs weak) based on 3D brain anatomical features has been introduced. A complete overview of the paper is shown in Fig. 1. Briefly, this work is organized as follows: Sec. II regards materials and methods, particularly, the dataset features, the pre-processing procedure and the applied machine learning (ML) approaches: random forest (RF), support vector machine (SVM) and logistic regression (LR). To support our analysis, in Sec. III, qualitative and quantitative comparisons and results, between the different adopted ML approaches are provided. The proposed approach has been evaluated on several MRI datasets by obtaining well-defined features that ultimately provide an average accuracy of 72% in the test set. As it is described in Sec. IV, motor-strength functions are effectively related to interesting and specific subsets of 3D brain regions. Thus, this work provides a novel and tested ensemble of machine learning methodologies to investigate and explain well-known and unknown relations between brain areas and motor-strength experiments.

II. Materials and Methods

In this work neurological and behavioral (motor-strength) experimental results are analyzed over thousands of subjects and for each of them, the experiments are carried out under the same conditions. The entire methodology is described in detail in the pipeline of Fig. 1. The results of these experiments consist of the collection of strong-weak labels associated to MRI data (see Fig. 1 *box A* and Sec. II-A). The cleaning of the process, the dataset normalization and splitting for testing, training, and validation are applied (see Sec. II-B and Fig. 1 *box B*). In Sec. II-D the three supervised ML approaches adopted for the feature selection are described (RF, SVM and LR). In Fig. 1 - *box D-1* shows four different types of brain anatomical measurements (Cortical Thickness, Mean curvature, Volume, and Area) (see Sec. II-A). In order to define the best applicable ML strategy, the analysis of the different types of brain anatomical features was carried out; the results can been seen in Sec. III and 1 - *box D-1*. Therefore, as it is shown in 1 - box D(2) all the ML results are validated by performing a permutation test (see Sec. II-D). In Sec. III, final

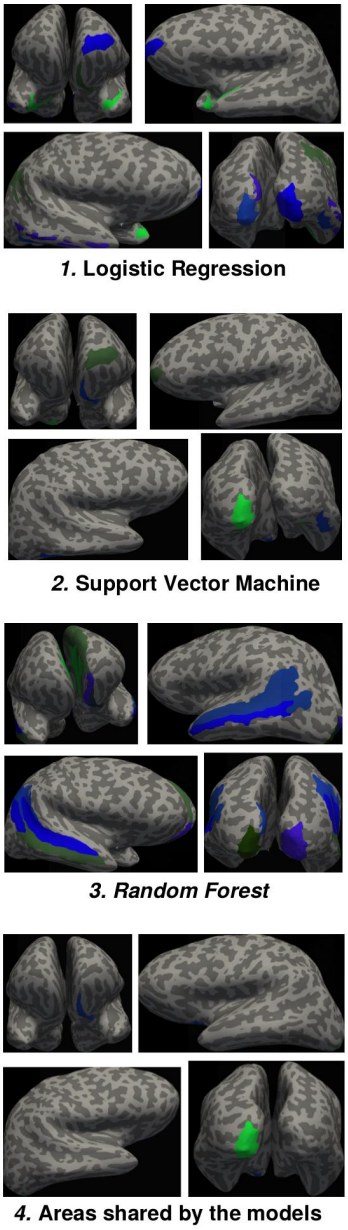

Fig. 2. 1-2-3 show the most significant areas obtained in each one of the ML approaches, LR, SVM, RF, respectively. 4 shows the area shared by the models.

results of the survey are commented and explained.

All the procedures are implemented with Python 3.7, using Scikit-learn [14], and Pandas packages [15]; the visualisation of the extracted ROIs in an inflated brain is performed using FreeSurfer 6.0 [16].

A. Dataset and experiment description

1) Neuroimaging collection and feature description: The dataset used in the experiments comes from the Human Connectome Project (S1200) (HCP), published on March 1, 2017; it includes behavioural information and (MRI) of 1206 healthy participants between age 22 - 35. moreover, 1113 of

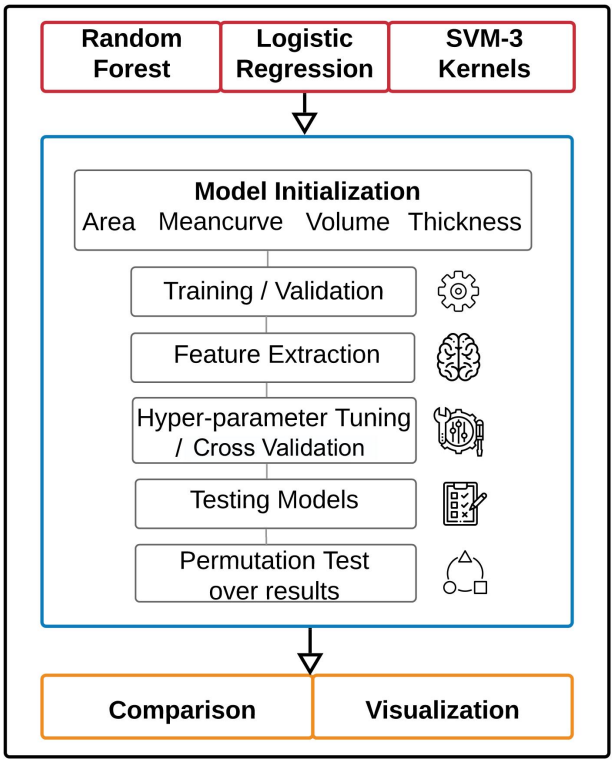

Fig. 3. General description of internal methodology applied in Fig. 1 Box **D-1 D-2** and textually explained in Sec. II-D. The red box shows the ML approaches used; all of them are inputs to the blue box. Blue box lists, for each ML approach step by step, how were the 4 models initialized, trained and validated, feature extraction applied to select the most significant ROIs, tested and finally approved by performing permutation test. The output of this box is the input for the orange box where the ultimate results are presented and visualised.

them present at least one three-dimensional (3D) T1-weighted (T1w) MRI scan [17], [18]. FreeSurfer reconstructs the brain surfaces starting from the 3D T1w MRI anatomical images and then extracts several measurements. For example, the cortical thickness that represents the distance between the gray/white matter boundary and the pial surface [19] and the cortical surface area that is the area covered by the cytoarchitectonic brain region over the external layer of cerebral cortex.

2) Motor-strength testing and label description: The strength analysis are performed with the *NIH toolbox* [20]: a comprehensive set of neuro-behavioral measurements that quickly assess cognitive, emotional, sensory, and motor functions [21]. For our study, we focused on the score of the Grip Strength test that indicates the strength in pounds that the participant can generate with a dynamometer. This testing procedure is validated by the American Society of Hand Therapists [22] and it requires approximately 3 minutes. During this procedure, the participants squeeze the Jamar Plus Digital dynamometer [23] three times with their dominant hand as hard as they can. The dynamometer provides a digital score of strength in pounds after it is adjusted to the age of the participants. Then, given this measurement for all the subjects involved in the dataset, a median value of the strength score

is computed. Furthermore, comparing the strength score for each subject with the median score value, each subject is either labeled as strong (label +1) or weak (label -1).

3) Final dataset: In Fig.1, box **A-B** the shape of the data-set is shown. In particular, for each patient a motor-strength binary label is associated to two different files generated with Freesurfer [24]. the 4 brain anatomical measurements of left and right hemisphere are collected in two files. In detail, these measurements are the area, volume, cortical thickness and mean curve of 74 brain regions per hemisphere. Summarizing, each record represents one of two hemispheres of the brain, 1113 subject, and 74 ROI based on the Destrieux Atlas [9].

B. Data preprocessing: cleaning of the sources, normalization and data-set splitting

One of the crucial steps for a correct data analysis relies in data preprocessing and normalization. In particular, in Fig. 1, Box **B** these steps are shown in a pipeline. The first step consists of removing missing data from the whole dataset resulting in a total of 1108 subjects. In the second step, the two files (which represent the two hemispheres) were merged in one file with 1108 rows (subjects) and 148 columns. In the third step, data were normalized according to the Z-score, in 1.

$$Z = \frac{x - \mu}{\sigma} \tag{1}$$

Finally, the dataset of all participants is split into training-set (50%) validation-set (30%) and test-set (20%). Each split has an approximate equally distributed number of samples for each label (50% of weak labels and 50% of strong labels).

C. Preliminary results and comparisons of brain anatomical measurements and their distributions

Before implementing any parametric test (e.g. correlation, analysis of variance or t-tests), it is necessary to check if data follows a normal distribution [25]. An Anderson-Darlings test [26] is applied to separate the ROIs with normal distribution and the ROIs with non-normal distribution; this step is essential to define if a parametric or not parametric test can be used for the separation of the features. For the ROIs with normal distribution, the t-test was applied to compare strong and weak subjects, in the other cases a Mann-Whitney U test [27] was performed. It is outlined that the separability of the classes are not significant from a statistical point of view, leading to the need of more advanced machine learning methods.

D. Application of ML approaches for classification and permutation tests

In this work, as it is shown in Fig. 1, box **C**, three different ML approaches were adopted. Particularly, our analysis were performed with Random Forest, Logistic Regression and Support Vector Machine. For all the models, a standard pipeline (see Fig. 3) of 6 steps is applied as follows: *(i)* for each ML approach, one model for each brain anatomical measurement is created, *(ii)* then, the models were trained with all the ROIs, *(iii)* and the accuracy was checked using the validation-set, *(vi)* next, feature-extraction was applied, *(v)* later, hyper-parameter tuning with cross-validation was performed to reduce the bias error and the variance, *(vi)* and, finally, each model was tested and validated with 10.000 permutation test on the predicted features. Thus, for each model, the reliability of the binary classifier is shown with an associated p-value.

1) Random Forest: RF models are applied both to extract essential ROIs and reduce the feature-set dimensionality (see also Fig. 1, box **C-1**). In particular, the output significance related to each ROI is computed as follows: sort the number of the ROIs in a descendent way with respect to their scores to find the feature combination which provides the best accuracy. Bias and the variance were reduced using the following hyper-parameters found after a search process:

- Number of trees in the forest (430).
- Maximum depth of the tree (50).
- Minimum number of samples required to be at a leaf node (9).
- The minimum number of samples required to split an internal node (6).

2) Support Vector Machine: SVM creates hyper-planes through a multidimensional space based on a window function also known as kernel function. The kernel function objective consists of obtaining a separation of the groups. In this work we used SVM with different kinds of kernels with linear, radial (Radial Basis Functions, RBF) and polynomial (see also Fig. 1 box **C-2**). For the feature extraction process recursive feature extraction was analysed. For each kernel function, a set of independent models is analysed. In Sec. II-D, the complete pipeline is described. The hyper-parameter configuration for the best models and listed below are shown in Table I in the case of the area features.

- The strength of the regularization (SR).
- Gamma coefficient for RBF and polynomial (G).
- Degree of the polynomial kernel function (D).

TABLE I
BEST SVM KERNELS HYPER-PARAMETERS CONFIGURATION FOR AREA BRAIN MEASUREMENT

SVM	SR	G	D
Linear	0.01	-	-
RBF	10	0.01	-
Poly	0.001	0.001	7

3) Logistic Regression: LR models [28] are probabilistic and supervised models. The weights are optimized using L1 regularization (also known as Lasso (see also Fig. 1 - box **C-3**). In particular, with the L1 regularization, the number of features is minimised, generating sparse models. In such a way, the results interpretability is facilitated and the parameter explosion is prevented. At the end of the process, hyper-parameter regularization strength is set equal to 0.035 in the case of the area brain measurement. Which is the best performing feature.

TABLE II
PREDICTION PERFORMANCE WITH ALL ROIS AND AFTER FEATURE SELECTION AND HYPER-PARAMETER TUNING.

SVM kernels

Linear	All ROIs	Train	Validation	Test	Mean	P-Value	N. Total ROIs
Area	0.67	0.73	**0.71**	**0.77**	**0.70 ± 0.03**	9.99×10^{-5}	**11**
Mean curve	0.63	**0.86**	0.64	0.64	0.62 ± 0.13	9.99×10^{-5}	89
Thickness	0.69	**0.77**	0.75	0.65	0.59 ± 0.06	1.0×10^{-4}	113
Volume	0.69	0.75	**0.71**	**0.68**	**0.69 ± 0.04**	9.99×10^{-5}	**14**
RBF							
Area	0.69	0.76	**0.70**	**0.77**	**0.73 ± 0.04**	9.99×10^{-5}	**11**
Mean curve	0.58	**0.83**	0.67	0.68	0.72 ± 0.09	9.99×10^{-5}	89
Thickness	0.59	**0.96**	0.64	0.64	0.70 ± 0.18	9.99×10^{-5}	113
Volume	0.70	0.76	**0.70**	**0.67**	**0.79 ± 0.05**	9.99×10^{-5}	**14**
Polynomial							
Area	0.66	0.70	**0.68**	**0.72**	**0.70 ± 0.02**	9.99×10^{-5}	**11**
Mean curve	0.67	**0.86**	0.63	0.64	0.61 ± 0.13	9.99×10^{-5}	89
Thickness	0.64	**0.65**	0.50	0.50	0.58 ± 0.09	1.0×10^{-4}	113
Volume	0.67	0.76	**0.72**	**0.69**	**0.75 ± 0.04**	9.99×10^{-5}	**14**

Random forest

	All ROIs	Train	Validation	Test	Mean	P-Value	N. Total ROIs
Area	0.72	0.71	**0.74**	**0.76**	0.74 ± 0.03	9.0×10^{-5}	**20**
Mean curve	0.68	0.68	0.67	0.70	0.68 ± 0.02	9.0×10^{-5}	45
Thickness	0.70	0.67	0.72	0.68	0.69 ± 0.03	9.0×10^{-5}	60
Volume	0.73	0.74	**0.75**	**0.71**	0.73 ± 0.02	9.0×10^{-5}	**20**

Logistic Regression (Lasso)

	All ROIs	Train	Validation	Test	Mean	P-Value	N. Total ROIs
Area	0.68	0.71	**0.72**	**0.73**	**0.72 ± 0.01**	9.0×10^{-4}	**20**
Mean curve	0.65	0.78	0.69	0.68	0.72 ± 0.06	9.0×10^{-4}	72
Thickness	0.68	0.76	0.74	0.65	0.72 ± 0.06	9.0×10^{-4}	56
Volume	0.69	0.78	**0.73**	**0.74**	**0.75 ± 0.03**	9.0×10^{-4}	**55**

III. DISCUSSION AND RESULTS

In this work, supervised ML approaches have been applied to predict and recognize brain anatomical measurements that correlate under a certain accuracy, in some ROIs of the human brain, with motor strength. For each ML approach the obtained results were validated by using permutations tests. As it is described in Sec. II-C, preliminary studies on feature distributions and traditional statistical analysis were performed. The preliminary studies show that the feature are not separable by using statistical tests. In detail, following the pipeline of Sec. II-A and shown in Fig. 3, the classification accuracy on the validation-set is obtained considering all the ROIs for each brain anatomical measurement. Then, feature extraction and hyper-parameter tuning were applied on the validation-set and tested in test-set. The results obtained from RF, SVM, and LR with their corresponding p-values (from the permutation tests) are summarized in Table II. In general, the anatomical brain measurements that have achieved a statistical relevant accuracy are *area* and *volume*. *Area* and *volume* present also a low variance reflecting their low accuracy fluctuation along the predictions. Furthermore, SVM approaches turn out to be a relevant example of how the hyperparameter tuning may improve the predictions and reduce the overfitting. In general, classification scores achieve a significant level of reliability for the ML approaches with p-values less or equal to 0.0009 (p-value $\leq 9 \times 10^{-4}$). The total number of selected ROIs after the hyperparameters tuning is shown in Table II. In particular, *area* and *volume* have the lowest number of ROIs with a high classification accuracy. The most significant ROIs shared by *volume* and *area* have been selected and displayed in Fig. 2, as projected into a 3-D brain model.

For each ML approach, significance ranked lists are shown in Table III. The ranking schema outlines the positions of *volume* and *area* summarizing the most important ROIs used for classification. For SVM, we reported the ROIs with respect to their relative frequencies in a decreasing order. An additional table is provided in which the results of the most significant ROIs among the different ML approaches are collected (Table III). The most significant ROIs in common between *volume* and *area* are projected into a 3-dimensional brain model, Fig. 2. Morphometric measurements like area and volumes of brain areas showed to be the most helpful features for all the classification approaches were presented. Therefore, it seems that size of the brain regions is a good discriminant for

TABLE III
MOST SIGNIFICANT BRAIN ROIS FOR AREA AND VOLUME.

Logistic Regression (Lasso)

	ROI Area	Significance	ROI Volume	Significance
1.	lh_S_orbital_med-olfact_area	0.14	lh_S_orbital_med-olfact_volume	0.08
2.	lh_G_and_S_frontomargin_area	0.09	lh_G_temp_sup-Plan_polar_volume	0.06
3.	lh_G_cuneus_area	0.09	lh_Pole_occipital_volume	0.04
4.	rh_Pole_occipital_area	0.08	lh_G_temp_sup-G_T_transv_volume	0.04
5.	lh_Pole_occipital_area	0.08	rh_S_temporal_inf_volume	0.04
6.	rh_G_pariet_inf-Angular_area	0.08	lh_G_and_S_frontomargin_volume	0.04
7.	lh_S_temporal_sup_area	0.08	rh_G_subcallosal_volume	0.03
8.	rh_S_oc-temp_lat_area	0.07	rh_S_collat_transv_post_volume	0.03
9.	lh_G_oc-temp_med-Parahip_area	0.05	rh_Pole_temporal_volume	0.03
10.	rh_G_occipital_sup_area	0.05	rh_Pole_occipital_volume	0.03
11.	rh_G_oc-temp_med-Parahip_area	0.03	rh_S_suborbital_volume	0.03
12.	lh_G_pariet_inf-Angular_area	0.03	rh_S_oc-temp_lat_volume	0.03
13.	rh_S_pericallosal_area	0.03	rh_S_orbital_med-olfact_volume	0.03
14.	lh_S_parieto_occipital_area	0.03	lh_G_cuneus_volume	0.03
15.	lh_S_circular_insula_sup_area	0.02	lh_G_orbital_volume	0.02
	Other ROIs were omitted with a total significance of:	0.06	Other ROIs were omitted with a total significance of:	0.41

Support Vector Machine

	ROI Area	Significance	ROI Volume	Significance
1.	lh_G_and_S_frontomargin_area	0.14	lh_S_orbital_med-olfact_volume	0.11
2.	lh_Pole_occipital_area	0.11	lh_G_temp_sup-Plan_polar_volume	0.11
3.	rh_S_oc-temp_lat_area	0.10	lh_Pole_occipital_volume	0.09
4.	lh_S_orbital_med-olfact_area	0.10	lh_G_orbital_volume	0.08
5.	rh_G_occipital_sup_area	0.10	rh_G_front_sup_volume	0.08
6.	rh_G_pariet_inf-Angular_area	0.09	lh_G_and_S_frontomargin_volume	0.08
7.	lh_S_circular_insula_sup_area	0.08	rh_G_and_S_cingul-Ant_volume	0.07
8.	rh_S_pericallosal_area	0.08	rh_S_oc-temp_lat_volume	0.07
9.	rh_S_front_sup_area	0.08	rh_G_subcallosal_volume	0.06
10.	lh_G_pariet_inf-Angular_area	0.07	lh_G_insular_short_volume	0.06
11.	rh_S_orbital-H_Shaped_area	0.06	lh_G_temp_sup-G_T_transv_volume	0.05
12.			rh_Pole_occipital_volume	0.05
13.			rh_S_collat_transv_post_volume	0.04
14.			rh_S_temporal_inf_volume	0.04

Random Forest

	ROI Area	Significance	ROI Volume	Significance
1.	rh_G_and_S_cingul-Ant_area	0.08	lh_S_orbital_med-olfact_volume	0.1
2.	rh_G_temporal_middle_area	0.06	rh_G_temporal_middle_volume	0.07
3.	rh_S_temporal_sup_area	0.06	lh_G_temp_sup-Plan_polar_volume	0.06
4.	lh_G_cuneus_area	0.06	lh_G_front_sup_volume	0.06
5.	lh_G_oc-temp_med-Parahip_area	0.06	lh_Pole_occipital_volume	0.05
6.	lh_S_temporal_sup_area	0.06	rh_S_temporal_inf_volume	0.05
7.	lh_G_front_sup_area	0.05	rh_S_oc-temp_lat_volume	0.05
8.	rh_G_occipital_sup_area	0.05	lh_G_rectus_volume	0.05
9.	lh_S_orbital_med-olfact_area	0.05	lh_G_temporal_middle_volume	0.05
10.	lh_Pole_occipital_area	0.05	lh_G_cuneus_volume	0.05
11.	rh_S_front_middle_area	0.05	rh_G_and_S_cingul-Ant_volume	0.05
12.	lh_G_rectus_area	0.05	rh_Pole_occipital_volume	0.05
13.	rh_Pole_occipital_area	0.05	lh_G_insular_short_volume	0.04
14.	rh_G_pariet_inf-Angular_area	0.04	lh_S_temporal_sup_volume	0.04
15.	lh_G_temporal_middle_area	0.04	rh_S_orbital_med-olfact_volume	0.04
	Other ROIs were omitted with a total significance of:	0.19	Other ROIs were omitted with a total significance of:	0.19

the motor-strength classification. However, none of the regions that showed to be statistically significant are in the motor cortex or are strictly related to the hand movement. Nonetheless, the Grip Strength test score has been recently proved to be a possible low-cost marker for the cognitive performance and overall brain health [29], [29]–[31]. Indeed, the brain regions that showed to be significant for the classification approaches are located mostly in frontal, temporal lobes that host many important high-order cognitive functions and in the occipital lobe that subserves the human vision. For instance, in the frontal lobes there are areas known to be involved in working memory and error detection; auditory and, more in general, language comprehension are functions related to the temporal lobe areas. Finally, in the occipital pole that has been shown to be common to all the models the visual system is located.

IV. Conclusion

A novel pipeline has been introduced to use supervised ML approaches for binary classification problems on anatomical brain data. The extraction and classification of the features were performed by using RF, LR with Lasso, SVM with three different kernels: Linear, RBF and Polynomial and traditional statistical methods. The results show that supervised ML approaches are a promising alternative to traditional statistical tests for the feature extraction and classification. In fact, they achieve high precision and low variance by reducing the dimensionality of data. Moreover, the benefits of the adoption of ML approaches in this domain are evident, not only in quantifiable increases in the performances, but also in qualitative aspects, such as higher reduction of overfitting. Regarding the brain areas observed for all the classification approaches, we cannot exclude that, as the Grip Strength score has been associated with brain health the classification approaches are detecting early anatomical differences or changes related to future impairments in cognitive functions. However, future behavioural, structural and functional MRI studies (longitudinal and non-longitudinal) are warranted to explore deeper this speculation and strongly corroborate the integration of machine learning techniques in neuroimaging studies.

References

[1] P. Galdi, M. Fratello, F. Trojsi, A. Russo, G. Tedeschi, R. Tagliaferri, and F. Esposito, "Consensus-based feature extraction in rs-fmri data analysis," *Soft Computing*, vol. 22, no. 11, pp. 3785–3795, 2018.

[2] M. Helmstaedter, "The mutual inspirations of machine learning and neuroscience," *Neuron*, vol. 86, no. 1, pp. 25–28, 2015.

[3] N. Chumerin and M. M. Van Hulle, "Comparison of two feature extraction methods based on maximization of mutual information," in *2006 16th IEEE Signal Processing Society Workshop on Machine Learning for Signal Processing*. IEEE, 2006, pp. 343–348.

[4] A. Hyvärinen, "New approximations of differential entropy for independent component analysis and projection pursuit," in *Advances in neural information processing systems*, 1998, pp. 273–279.

[5] J. M. Leiva-Murillo and A. Artes-Rodriguez, "Maximization of mutual information for supervised linear feature extraction," *IEEE Transactions on Neural Networks*, vol. 18, no. 5, pp. 1433–1441, 2007.

[6] E. Parzen, "On estimation of a probability density function and mode," *The annals of mathematical statistics*, vol. 33, no. 3, pp. 1065–1076, 1962.

[7] A. Kraskov, H. Stögbauer, and P. Grassberger, "Estimating mutual information," *Physical review E*, vol. 69, no. 6, p. 066138, 2004.

[8] K. E. Hild, D. Erdogmus, K. Torkkola, and J. C. Principe, "Feature extraction using information-theoretic learning," *IEEE Transactions on Pattern Analysis and Machine Intelligence*, vol. 28, no. 9, pp. 1385–1392, 2006.

[9] C. Destrieux, B. Fischl, A. Dale, and E. Halgren, "Automatic parcellation of human cortical gyri and sulci using standard anatomical nomenclature," *Neuroimage*, vol. 53, no. 1, pp. 1–15, 2010.

[10] B. Mwangi, T. S. Tian, and J. C. Soares, "A review of feature reduction techniques in neuroimaging," *Neuroinformatics*, vol. 12, no. 2, pp. 229–244, 2014.

[11] L. Lavagnino, F. Amianto, B. Mwangi, F. D'Agata, A. Spalatro, G. Zunta-Soares, G. A. Daga, P. Mortara, S. Fassino, and J. Soares, "Identifying neuroanatomical signatures of anorexia nervosa: a multivariate machine learning approach," *Psychological medicine*, vol. 45, no. 13, pp. 2805–2812, 2015.

[12] J. Akhila, C. Markose, and R. Aneesh, "Feature extraction and classification of dementia with neural network," in *2017 International Conference on Intelligent Computing, Instrumentation and Control Technologies (ICICICT)*. IEEE, 2017, pp. 1446–1450.

[13] K. Shen, X. Li, W. Pullens, H. Zheng, C. Ong, and E. Wilder-Smith, "Key feature extraction for fatigue identification using random forests," in *2005 IEEE Engineering in Medicine and Biology 27th Annual Conference*. IEEE, 2006, pp. 2044–2047.

[14] F. Pedregosa, G. Varoquaux, A. Gramfort, V. Michel, B. Thirion, O. Grisel, M. Blondel, P. Prettenhofer, R. Weiss, V. Dubourg, J. Vanderplas, A. Passos, D. Cournapeau, M. Brucher, M. Perrot, and E. Duchesnay, "Scikit-learn: Machine learning in Python," *Journal of Machine Learning Research*, vol. 12, pp. 2825–2830, 2011.

[15] W. McKinney *et al.*, "pandas: a foundational python library for data analysis and statistics," *Python for High Performance and Scientific Computing*, vol. 14, no. 9, 2011.

[16] M. Reuter, N. J. Schmansky, H. D. Rosas, and B. Fischl, "Within-subject template estimation for unbiased longitudinal image analysis," *Neuroimage*, vol. 61, no. 4, pp. 1402–1418, 2012.

[17] D. Marcus, J. Harwell, T. Olsen, M. Hodge, M. Glasser, F. Prior, M. Jenkinson, T. Laumann, S. Curtiss, and D. Van Essen, "Informatics and data mining tools and strategies for the human connectome project," *Frontiers in neuroinformatics*, vol. 5, p. 4, 2011.

[18] D. M. Barch, G. C. Burgess, M. P. Harms, S. E. Petersen, B. L. Schlaggar, M. Corbetta, M. F. Glasser, S. Curtiss, S. Dixit, C. Feldt *et al.*, "Function in the human connectome: task-fmri and individual differences in behavior," *Neuroimage*, vol. 80, pp. 169–189, 2013.

[19] B. Fischl and A. M. Dale, "Measuring the thickness of the human cerebral cortex from magnetic resonance images," *Proceedings of the National Academy of Sciences*, vol. 97, no. 20, pp. 11 050–11 055, 2000.

[20] R. C. Gershon, M. V. Wagster, H. C. Hendrie, N. A. Fox, K. F. Cook, and C. J. Nowinski, "Nih toolbox for assessment of neurological and behavioral function," *Neurology*, vol. 80, no. 11 Supplement 3, pp. S2–S6, 2013.

[21] D. B. Reuben, S. Magasi, H. E. McCreath, R. W. Bohannon, Y.-C. Wang, D. J. Bubela, W. Z. Rymer, J. Beaumont, R. M. Rine, J.-S. Lai *et al.*, "Motor assessment using the nih toolbox," *Neurology*, vol. 80, no. 11 Supplement 3, pp. S65–S75, 2013.

[22] "American Society of Hand Therapists (ASHT)." [Online]. Available: https://www.asht.org/

[23] B. R. Niebuhr, R. Marion, and M. L. Fike, "Reliability of grip strength assessment with the computerized jamar dynamometer," *The Occupational Therapy Journal of Research*, vol. 14, no. 1, pp. 3–18, 1994.

[24] H. WU-Minn, "1200 subjects data release reference manual," *URL https://www. humanconnectome. org*, 2017.

[25] A. Ghasemi and S. Zahediasl, "Normality tests for statistical analysis: a guide for non-statisticians," *International journal of endocrinology and metabolism*, vol. 10, no. 2, p. 486, 2012.

[26] G. W. Corder and D. I. Foreman, "Nonparametric statistics for non-statisticians," 2011.

[27] Ö. Öztürk and D. A. Wolfe, "An improved ranked set two-sample mann-whitney-wilcoxon test," *Canadian Journal of Statistics*, vol. 28, no. 1, pp. 123–135, 2000.

[28] P. Lodha, A. Talele, and K. Degaonkar, "Diagnosis of alzheimer's disease using machine learning," in *2018 Fourth International Conference on Computing Communication Control and Automation (ICCUBEA)*. IEEE, 2018, pp. 1–4.

[29] J. Firth, B. Stubbs, D. Vancampfort, J. A. Firth, M. Large, S. Rosenbaum, M. Hallgren, P. B. Ward, J. Sarris, and A. R. Yung, "Grip strength is associated with cognitive performance in schizophrenia and the general population: a uk biobank study of 476559 participants," *Schizophrenia bulletin*, vol. 44, no. 4, pp. 728–736, 2018.

[30] R. McGrath, S. G. Robinson-Lane, S. Cook, B. C. Clark, S. Herrmann, M. L. O'Connor, and K. J. Hackney, "Handgrip strength is associated with poorer cognitive functioning in aging americans," *Journal of Alzheimer's Disease*, vol. 70, no. 4, pp. 1187–1196, 2019.

[31] N. S. Ward, J. M. Newton, O. B. Swayne, L. Lee, R. S. Frackowiak, A. J. Thompson, R. J. Greenwood, and J. C. Rothwell, "The relationship between brain activity and peak grip force is modulated by corticospinal system integrity after subcortical stroke," *European Journal of Neuroscience*, vol. 25, no. 6, pp. 1865–1873, 2007.